SPACE TELESCOPE SCIENCE INSTITUTE
Operated for NASA by AURA

Instrument Science Report COS 2013-07

COS/FUV Spatial and Spectral Resolution at the new Lifetime Position

Julia Roman-Duval[1], Erin Elliott[1], Alessandra Aloisi[1], Tom Delker[2], Cristina Oliveira[1], Rachel Osten[1], Steve Osterman[3], Steve Penton[1], and Paule Sonnentrucker[1]

[1] Space Telescope Science Institute, Baltimore, MD
[2] Ball Aerospace
[3] University of Colorado, Boulder

June 10, 2013

ABSTRACT

In order to overcome gain-sag effects, the default position of spectra on the COS FUV detector was recently moved by 3.5" in the positive cross-dispersion direction, and by −0.05" in the dispersion direction. This move to the second "lifetime position", a fresh part of the detector which has not yet experienced significant gain sag, is potentially accompanied by changes in flux calibration, sensitivity, flat-field, and resolution. Hence, special calibration programs were undertaken to characterize the detector at this new lifetime position. In this ISR, we characterize the spatial and spectral resolution at the second COS FUV lifetime position. Code V Optical models of the COS LSFs are generated for modes of the M and L gratings, accounting for mid-frequency wavefront errors (MFWFE). In order to validate the modeling of the COS FUV LSFs, we perform a comparison of spectral line profiles between, on the one hand, COS FUV spectra of SMC O star AV75 acquired at the second lifetime position, and on the other hand previous STIS E140M spectra convolved with models of the COS FUV LSFs at the new lifetime position. Our analysis shows that the model LSFs are consistent with the observations within the measurement errors. In addition, we derive the spatial resolution of the COS FUV gratings at the new lifetime position, as a function of wavelength, from both observations and optical modeling. We show that the theoretical and observed cross-dispersion profiles are in very good agreement.

1. Introduction

A limited amount of charge can be extracted from the FUV cross-delay lines of COS. As a result, the gain in a pixel — the number of electrons generated by the photon — decreases as the cumulative number of photons ever collected in that pixel increases. This effect, known as "gain-sag", leads to a localized loss of sensitivity with time. When the modal gain — defined as the peak of the gain distribution — becomes lower than about 2, the flux in that pixel cannot be recovered.

On July 23rd, 2012, the default location of COS FUV spectra was shifted to lifetime position 2, LP2, by 3.5" in the cross-dispersion direction, and by -0.05" along the dispersion direction relative to the original lifetime position, or lifetime position 1 (LP1). This change in "lifetime position" aimed at mitigating "gain-sag" effects in the COS FUV detector by positioning science spectra on a fresh, previously un-illuminated part of the detector, where little to no charge has been extracted and the gain is at its nominal value. The selection of this lifetime position 2 was optimized to maximize spectral resolution, minimize the effects of gain-sag from previously exposed regions, and maximize the number of remaining future lifetime positions.

Because the lifetime move involved a change in the optical path of FUV photons, changes in spectral and spatial resolution are correspondingly expected. Thus, the resolution of the COS FUV modes at the second lifetime position needed to be calibrated. The COS Line Spread Functions (LSFs) are known to be non-gaussian due to mid-frequency wavefront errors (MFWFE), which are polishing errors on the primary and secondary HST mirrors (COS ISR 2009-01). Because the wings of the COS LSFs contain a significant fraction of the total power, a proper characterization of the COS LSFs is necessary to perform accurate line profile fitting, and to determine the feasibility and required exposure time of weak and/or narrow spectral features. While the contributions from MFWFE have remained the same with the COS FUV lifetime move, the LSFs resulting from the COS+OTA (optical telescope assembly) combination have changed.

We have modeled the COS FUV LSFs and cross-dispersion (XD) profiles at LP2 using a code V optical model, and validated the model using observations with the COS FUV gratings at lifetime position 2. These observations were taken as part of several Cycle 19 special calibration programs: FCAL2 (12805, PI: Roman-Duval), which aimed at characterizing the spectral resolution and dispersion solution of the FUV M gratings at LP2; FCAL3 (12806, PI: Massa), which aimed at calibrating the sensitivity and flat fields at LP2; and FENA3 (12796, PI: Oliveira), which determined the optimal focii at the new position. While the FCAL2 observations were obviously used to validate the model LSFs of the M gratings at LP2, the FENA3 observations were used to characterize the spectral resolution of the G140L at LP2, and the FCAL3 exposures were used to empirically determine the spatial resolution, and to validate the model XD profiles of all FUV gratings at LP2.

In this ISR, we describe the complete analysis of the COS FUV spectral and spatial resolution at the new lifetime position. The comparison of the FUV spectral and

spatial resolution between LP1 and LP2 will be discussed in a separate ISR. The characterization of the spectral and spatial resolution of the new FUV cenwaves (G130M/1055, 1096, and 1222) will be also be presented in a future ISR.

2. Model of the COS LSFs at lifetime position 2

The Line Spread Functions (LSF) of all COS FUV settings at the second lifetime position were modeled using code V, based on a model of the COS system provided by Tom Delker (Ball Aerospace) and updated by Erin Elliott. The move to the second lifetime position incurred a change in field angle. Hence, pointing was adjusted to +3.5 arcsec in the +YUSER direction in COS coordinates. This was done by adding + 3.5 arcsec and −0.05 arcsec shifts in the cross-dispersion and dispersion directions to the original design field point, given by $\mathrm{X}_{CodeV} = \mathrm{X}_{user} = -0.000725°$, $\mathrm{Y}_{CodeV} = \mathrm{Y}_{user} = 0.089939°$.

All PSFs for the COS system are highly astigmatic. The grating positions (focus, rotation) are chosen so that the PSF on the image plane is as narrow as possible in the dispersion direction, to maximize the spectral resolution of the system. The grating positions are specified by giving the motor step numbers for the focus motor and the rotation motor. Each step of the rotation motor leads to a 0.028125°change in grating tilt, while each step of the focus motor leads to a 2.35185 μm change in the linear (focus) position of the grating.

The rotation position values were updated according to Table 1 at lifetime position 2. A rotation of the grating incurs a focus shift in the grating as well. The focus then must be independently set with the linear focus stage. The optimal focus values of each FUV mode at the second lifetime position were empirically determined in COS ISR 2013-01 (Oliveira et al., 2013), and propagated in the code V model at lifetime position 2, as shown in Table 2. The different shifts in focus incurred by the grating rotation and the adjustment of the linear focus stage were calculated as follows. The tilt position for each mode, α, corresponding to the updated grating rotation and focus, is calculated as the number of rotation steps N_R from nominal (N_{R_0}) times the rotation step size (ΔR), plus the nominal tilt location of the grating, α_0:

$$\alpha = (N_R - N_{R_0}) \times \Delta R + \alpha_0 \tag{1}$$

The focus shift, f_{total}, is the sum of two parts: the focus shift due to the linear stage, f_F, and the focus shift due to the rotation motion, f_R: $f_{\mathrm{total}} = f_F + f_R$. The focus shift due to the linear stage is calculated as the number of focus steps N_F from nominal N_{F_0} times the motor step size, ΔF:

$$f_F = (N_F - N_{F_0}) \times \Delta F \tag{2}$$

The focus shift due to a motion of the rotary stage is calculated as:

$$f_R = -42.8 \times (N_R - N_{R_0}) \times \Delta F \tag{3}$$

The updated code V focus values at lifetime position 2 are shown in Table 2.

Grating	Central wavelength Å	Rotation motor steps	Rotation motor steps from nominal	code V tilt value °
G130M	1291	7999	8	-19.875000
	1300	7995	4	-19.987500
	1309	7991	0	-20.100000
	1318	7987	−4	-20.212500
	1327	7983	−8	-20.325000
G160M	1577	11203	8	-19.875
	1589	11199	4	-19.9875
	1600	11195	0	-20.1
	1611	11191	−4	-20.2125
	1623	11187	−8	-20.325
G140L	1105	1598	7	-7.2105
	1230	1591	0	-7.4074
	1280	1590	−1	-7.4355

Table 1.: *Tilt values for the COS FUV gratings at lifetime position 2*

Grating	Central wavelength Å	Focus shift incurred by tilt motion (mm)	Focus motor step #	# of focus steps from nominal	Focus shift due to focus stage (mm)	total focus shift (mm)
G130M	1291	0.805	−50	− 220	0.517	1.322680
	1300	0.403	120	− 50	0.118	0.520229
	1309	0	290	120	−0.282	−0.282222
	1318	−0.403	460	290	−0.682	− 1.084673
	1327	−0.805	631	461	−1.084	−1.889476
G160M	1577	0.805	−224	−180	0.423	1.229
	1589	0.403	−54	−10	0.024	0.426
	1600	0.	116	160	−0.376	0.376
	1611	−0.403	286	330	−0.776	−1.179
	1623	−0.805	456	500	−1.176	−1.981
G140L	1105	0.705	−535	−505	1.188	1.892
	1230	0	−195	−165	0.388	0.388
	1280	−0.101	−146	−116	0.273	0.172

Table 2.: *Focus values for the COS FUV modes at lifetime position 2*

In addition to the update in rotation, focus, and field angle required by the move to lifetime position 2, the COS FUV LSFs described here include the following improve-

ments compared to the model at LP1 described in Ghavamian et al. 2009 (COS ISR 2009-01):

- Surface errors, which determine the PSF shape of the system at the short wavelengths used by the COS instrument, were added to the primary and secondary mirrors. Surface error maps were provided by Lallo, and are the same surface maps used in the TinyTim software (Krist et al., 2011).
- Apertures were added on the image plane surface that encompass the active detector areas. To locate the apertures in approximately the correct location, the G130M-1309 mode was used at the first lifetime position. The four wavelengths limiting each segment of the COS FUV detector (Table 3) were used to locate the detector apertures to the correct location, to within about 0.1 mm. The wavelength ranges were then verified to fall at the edges of the apertures for the other modes. Since the aperture location is not grating or cenwave dependent, only one mode (G130M/1309) was used to locate the apertures.
- The dispersion values of the gratings from the initial code V model were adjusted slightly to match values of wavelength ranges measured on the detectors during ground testing of the flight instrument (Tom Delker, private communication)

Grating	Central wavelength Å	Segment B		Segment A	
		Low	High	Low	High
G130M	1291	1129	1261	1284	1426
	1300	1139	1280	1295	1436
	1309	1149	1290	1305	1446
	1318	1158	1299	1314	1455
	1327	1168	1309	1324	1465
G160M	1577	1386	1559	1577	1751
	1589	1397	1571	1589	1762
	1600	1409	1581	1601	1774
	1611	1420	1594	1612	1786
	1623	1432	1606	1625	1798
G140L	1105	HV OFF		1118	2551
	1280	≤ 900	1165	1280	1391

Table 3.: *Wavelength ranges of the COS FUV gratings from the LP1 optical model*

Finally, Point Spread Functions (PSFs) were generated in Code V. For each grating mode, wavelengths were sampled every 50 Å (100 Å for the G140L). Each PSF file was a 1024 x 1024 array, with a physical pixel size of 2 x 2 μm. The raw PSFs were imported into Mathematica and converted to 6 x 24 μm pixels. Detector blur was then added by convolving the PSF array with a Gaussian kernel with $\sigma_x = 2$ pixels (12 μm) in

the dispersion direction, and $\sigma_y = 1$ pixel (24 μm) in the cross-dispersion direction. All PSF arrays were then normalized so that they contained the same total intensity. Finally, the arrays were summed along the cross-dispersion direction to generate the final Line Spread Function. All LSFs were normalized to have an integral of 1. The COS FUV LSFs at lifetime position 2 are shown in Figure 1.

3. Validation of the model LSFs using COS FUV observations

3.1 Requirements, goal, and design of the calibration observations

Characterizing the LSFs of the FUV gratings is essential for accurate line profile fitting, and to determine the feasibility and required exposure time of certain observations. The optical model presented in Section in principle fully characterizes the spectral resolution at LP2. However, it is necessary to test and validate this model using observations at LP2.

Two approaches were considered to perform this test: a direct and an indirect measurement of the COS LSFs. In the first case, the LSFs would be derived directly from the shape of unresolved spectral lines. This would require observations of numerous unresolved (and therefore ISM, not stellar) spectral lines with high signal-to-noise, and with sufficient coverage across the wavelength range of the G130M and G160M gratings. However, the paucity and weakness of unresolved ISM lines precluded such observations. Hence, we took an indirect approach, similar to the work done during SMOV on the COS spectral resolution at LP1 (Ghavamian et al., 2009, COS ISR 2009-01). In order to test the COS FUV LSF models at LP2, the adopted strategy consisted in comparing line profiles (both unresolved, resolved, and saturated) observed in COS FUV spectra obtained at lifetime position 2 with line profiles present in previous STIS high resolution echelle E140M spectra, and convolved with the model COS FUV LSFs at LP2. The comparison of synthetic and observed unresolved and saturated complex line profiles allowed us to constrain the changes in the core and wings of the LSF respectively.

After examining numerous reddened stellar spectra in the Milky Way and Magellanic Clouds, the SMC star AzV 75, an O5 III star, was chosen as the target of observations aimed at characterizing the spectral resolution of the FUV M gratings at LP2. AzV 75 was chosen for the following reasons: 1) it is in the appropriate brightness range for COS, not exceeding the local or global count rate, and yet allowing a high signal-to-noise to be reached relatively quickly; 2) it is one of the most reddened stars in the Tumlinson et al. (2002) catalog of Magellanic Cloud reddened stars observed by FUSE, with E(B-V) = 0.16. These conditions ensure the presence of numerous ISM lines, unresolved and saturated.

We performed a simple simulation to determine the S/N required in the observations to validate the model LSFs at LP2, based on the assumption that calibration observations aimed at validating the LP2 optical model should allow us to detect a change

in spectral resolution similar to the difference in spectral resolution between LP1 and LP2, which is of order 10% in the FWHM of the LSFs. Thus, we convolved the existing STIS E140M spectrum of AzV 75 with the model COS FUV LSFs at LP1 (described in Ghavamian et al. 2009) and at LP2. Since the convolution effectively removes noise in the convolved STIS spectra (see Figure 2), we then added random gaussian noise with varying S/N to the convolved spectra, and determined for which S/N differences in the simulated line profiles could be detected at a significant level. Note that the computations of the model LSFs at LP1 and LP2 are different, the LP2 model being improved compared to the LP1 model (see Section). As a result, changes between LP1 and LP2 in the shape of synthetic profiles obtained from the convolution of STIS spectra with model LSFs include contributions from both the lifetime move and improvements in the optical model. Nonetheless, the comparison of synthetic profiles between LP1 and LP2 gives a good constraint on the S/N required to detect subtle differences in spectral resolution.

According to the optical model, the change in spectral resolution between LP1 and LP2 affects mostly the core of the LSF. However, observations aimed at validating the model should allow us to detected unexpected changes in the wings of the LSFs. In order to determine the S/N required to detected a change of 15% in the wings of the LSFs, we performed a different simulation: we convolved the existing STIS E140M spectrum of AzV 75 with the model COS FUV LSFs at LP1 broadened uniformly by 15%, and added noise with varying S/N to the convolved spectra.

These two simulations showed that 1) a change of $\simeq 10\%$ in the core (FWHM) of the COS LSFs, similar to the difference between model LSFs at LP1 and LP2, could be detected with S/N = 60 per resolution element on the continuum in unresolved spectral lines (Figure 2, top panel), and 2) that a uniform broadening of 15% in the wings of the LSFs could be detected with S/N = 60 on the continuum in complex saturated profiles (Figure 2, bottom panel) .

For the M gratings, no data was available to validate the optical model. Hence, a special calibration program, FCAL2, aimed at characterizing the spectral resolution of the FUV M gratings, was required. We designed FCAL2 exposures to reach S/N = 60 on the continuum across the wavelength range of the M gratings, in order to be able to detect the subtle resolution changes between LP1 and LP2, and unexpected changes of order 10% or more. In addition, the spectral resolution of COS FUV varies with wavelength much more than with cenwave. In order to probe the LP2 spectral resolution across the wavelength range of the M gratings, FCAL2 included observations with the extreme cenwaves of each grating: the 1291 and 1327 for the G130M, and the 1577 and 1623 for the G160M.

To validate the G140L LSFs, high S/N observations of AzV 75 were already available from the FENA3 (12796, PI: Oliveira) lifetime enabling program. As a result, we did not acquire G140L observations as part of FCAL2.

3.2 Data

Program 12805 (FCAL2) obtained exposures with the G130M 1291 (1600s), 1327 (1400s), G160M 1577 (3000s) and 1623 (3500s) settings. In each case, the total exposure time was split equally amongst 4 FP-POS to maximize the S/N of the combined spectra. The program was packed into 4 orbits. The first orbit of the program, including the G130M/1291 exposures successfully executed on July 26, 2012. However, a guide star re-acquisition failure resulted in the loss of subsequent observations with the G130M/1327 and the G160M (1577 and 1623 settings). The latter observations were repeated successfully on September 11, 2012 during a 3 orbit visit. Table 4 lists all the FCAL2 (12805) exposures used in this analysis.

The calibrated data (x1d spectra) were retrieved from the archive. For each cenwave, the spectra obtained at different FP-POS were co-added using the FP-POS iterative algorithm developed by Ake et al. (2010) in order to remove fixed pattern noise. This algorithm has proven to work well with early type stars (AzV 75 is an O5 III star in the SMC) due to the smooth, un-crowded nature of their spectra. We verified that using this algorithm indeed improved the S/N compared so a simple co-addition, and did not produce artifacts in the final spectrum.

The G140L observations of AzV 75 were acquired as part of enabling program FENA3 ("Second COS FUV Lifetime Position: Focus Sweep Enabling Program FENA3", PID: 12796, PI: C. Oliveira), which aimed to determine the optimal focus of the G140L at the second lifetime position. The G140L observations consisted in 200s exposures at varying focii with the 1105 cenwave. The optimal focus was found to be at -535 motor steps (-165 from LP1), and corresponds to exposure lbx503kpq, which is used for this analysis.

The STIS E140M spectra used in this analysis, with resolution R $\simeq$ 45,000 and covering the wavelength range 1100 Å — 1700 Å , were obtained as part of program 7437 (PI: Lennon), and retrieved from the MAST archive (exposures o4wr11010 and o4wr11020). STIS echelle spectra directly retrieved from the archive exhibit large spikes at regular intervals, which result from the combination of the different orders. In order to mitigate this issue, we combined the echelle orders ourselves, and then co-added the two x1d spectra by weighing each exposure with the corresponding exposure times (2448 s and 3168 s respectively). The S/N of the combined spectrum varies between 10 and 20 per pixel across the wavelength range of the E140M at cenwave 1425. In the following analysis, we use this final co-added STIS spectrum.

3.3 Method

To construct synthetic COS G130M/1291, G130M/1327, G160M/1577, G160M/1623 spectra, and G140L/1105 spectra, we convolved the STIS spectrum with the corresponding model COS LSFs. First, the STIS spectrum was resampled on a wavelength grid with spacing equal to the COS dispersion: 9.97 mÅ, 12.21 mÅ, and 80.3 mÅ for the G130M, G160M, and G140L respectively. Second, the convolution was performed. The

Grating	Cenwave	Exposure	FP-POS
G130M	1291	lbxk01c2q	1
		lbxk01c4q	2
		lbxk01c6q	3
		lbxk01c8q	4
	1327	lbxk51kpq	1
		lbxk51ktq	2
		lbxk51kvq	3
		lbxk51kzq	4
G160M	1577	lbxk51l1q	1
		lbxk51l5q	2
		lbxk51lbq	3
		lbxk51ldq	4
	1623	lbxk51lfq	1
		lbxk51lhq	2
		lbxk51lmq	3
		lbxk51ltq	4

Table 4.: *Exposures from 12805 used in the characterization of the spectral resolution of the COS FUV M gratings.*

COS LSFs are sampled every 50 Å for the M gratings, and every 100 Å for the G140L. The shape of the LSF varies with wavelength, as seen in the FWHM measured in the model LSFs (Figure 1). Hence, we split the resampled STIS spectrum in the corresponding number of wavelength intervals closest to each of the wavelength of the grid of COS LSFs, and applied the convolution to each interval using the appropriate LSF. The convolution algorithm used the IDL routine CONVOL with the NORMALIZE and EDGE_TRUNCATE keywords.

We identified numerous ISM lines in the G130M, G160M, and G140L spectra to compare line profiles of synthetic and observed COS spectra at each of the extreme cenwaves of the G130M, G160M, and G140L gratings. The observed COS spectra are affected by small seemingly random shifts in wavelength between different cenwaves. Although these shifts, typically of magnitude $\pm$ 30 mÅ (or 3 pixels), do not violate the accuracy requirements of the wavelength solution (see Sonnentrucker et al. 2013), they are large enough to appear very obvious when comparing spectra taken at different cenwaves. If left uncorrected, they can cause significant line smearing. In each spectral window, we therefore determined by eye the wavelength shift to be applied to each of the two cenwaves of each grating in order to be aligned with the STIS spectrum, which has a better wavelength calibration that the COS spectrum (the STIS/E140M wavelength scale is accurate to within 3 mÅ, versus 30 mÅ for COS). In addition, we verified that there was no wavelength offset between spectra taken at one cenwave but different FP-POS.

Finally, we compared the synthetic ($f_s(\lambda)$) and observed ($f_o(\lambda)$) COS spectra in each spectral window, and computed the residual as $r(\lambda) = (f_o(\lambda) - f_s(\lambda))/f_s(\lambda)$.

While in principle the STIS echelle spectra should be de-convolved before applying the convolution with the COS LSFs, the large difference in spectral resolution between the STIS E140M grating (R $\simeq$ 45, 000) and the COS M (R $\simeq$ 20,000), and even more so COS L (R $\simeq$ 2,500), gratings is such that we can safely omit this difficult step. Indeed, the contribution from the STIS E140M FWHM would then only be at most 5% of the FWHM of the STIS E140M spectrum convolved with the COS M grating LSFs.

3.4 Results

The comparison between synthetic and observed COS spectra are shown in Figures 3, 4, 5, 6, and 7 for the G130M/1291, G130M/1327, G160M/1577, G160M/1623, and G140L settings respectively. The black line indicates the STIS E140M spectrum, the green lines show the synthetic COS spectra, obtained from the convolution of the STIS E140M spectrum with the model COS LSFs, and the red lines correspond to the observed COS spectra, binned by 5 pixels. Figures 3, 4, 5, 6, and 7 also show the fractional residual, which, in most cases, does not exceed 10%. There are some excursions to high fractional residual, but these are located in regions with very low counts, where the fractional residual is not well defined anyway.

Narrow, unresolved lines constrain the core (or FWHM) of the LSF best. On the other hand, the non-gaussian wings of the COS LSFs are better revealed in complex or blended, saturated wide profiles. Figures 3, 4, 5, 6, and 7 show that the model of the core and wings of the COS LSFs matches the observations very well: the fractional residual is within the error bars in all unresolved ISM lines. Note that the fractional residual in the bottom of saturated profiles, where the count rate is very low, is meaningless.

4. Characterization of the spatial resolution

4.1 Model of the COS cross-dispersion profiles

The optical model described in Section also yielded models of the cross-dispersion profiles of the COS FUV gratings as a function of wavelength. These were obtained by summing the model PSFs along the dispersion direction. The models are shown in Figures 8, 9, and 10 for the G130M, G160M, G140L gratings, respectively.

4.2 Data and Method

The move to the second lifetime position also incurred a change in spatial resolution: the cross-dispersion (XD) profiles are expected (and observed) to be narrower at the second lifetime position than they were at the original lifetime position. In order to verify that the changes in spatial resolution at LP2 were within the expectations, we have examined the spatial resolution at LP2, measured as the FWHM of the cross-dispersion profiles. In addition, we have compared the XD profiles observed at LP2 with model XD profiles derived from the optical model described in Section .

For this purpose, we used COS FUV data obtained as part of calibration program 12806/FCAL3 (COS FUV Lifetime Position: Flux and Flat Field Calibration and TDS transfer, PI: Massa). The program 12806 was designed to acquire spectra of white dwarves, which are smooth continuum sources with few stellar and ISM lines. Observations within 12806 were obtained using all cenwaves of the G130M, G160M, and G140L, and all FP-POS, at lifetime position 2. For some cenwaves, the LP2 observations include two exposures per FP-POS, and we use both of those exposures in this analysis in order to maximize the S/N. The paucity of spectral lines in the target spectra makes those data the ideal set to examine the spatial resolution at LP2. A list of FCAL3 exposures used to characterize the spatial resolution of the COS FUV gratings is included in Table 5.

4.3 Results

First, we have derived the FWHM of the observed XD profiles at LP2 as a function of grating, cenwave, and wavelength. The geometrically corrected, flat-fielded images (_flt file) of the M (resp. L) spectra were binned by 100 pixels (resp. 500 pixels) along the dispersion direction to obtain XD profiles as a function of wavelength, sampled every 50 (resp. 250) pixels. For each exposure and wavelength bin, a gaussian was fit to the corresponding XD profile to determine its center and FWHM. In some cases, a gaussian may not be the best representation of the XD profiles. Nonetheless, a gaussian fit provides a straight-forward measurement of the FWHM of the profiles. For a given cenwave, and in a given wavelength bin, the different values of the FWHM obtained from exposures taken at different FP-POS were then averaged together. The results of this analysis are shown in Figure 11 for all FUV gratings.

Second, we compared observed and model XD profiles at LP2, to verify the accuracy of the optical model described in Section . The model XD profiles are sampled at 6-16 wavelengths depending on the grating and cenwave combination. For each of those wavelengths λ_0, we computed the XD profile observed in the FCAL3 data by first identifying in the _x1d spectrum the detector column x_0 corresponding to that wavelength λ_0, and second by binning the image spectrum along the dispersion direction by 1000 pixels around x_0. We performed this analysis for each grating, cenwave, and FP-POS. The results are shown in Figures 8, 9, and 10 for the G130M, G160M, and G140L

respectively. The dashed lines indicate the model XD profiles at particular wavelengths, the solid lines correspond to the observed XD profiles at that wavelength, with each color corresponding to a different FPPOS. The FWHM of each XD profile are indicated in the panels.

Overall, there is a very good agreement between the model and observed XD profiles, typically to within a fraction of a pixel. Only for the G130M/1309 at 1450 Å does the model and observed XD profiles significantly deviate. However, the 1450 wavelength is located at the very edge of segment A for this setting, making the observed spectra at this location susceptible to large geometric distortions. Larger deviations from the model XD profiles are observed for the G140L, particularly for the 1105 cenwave at 1300 Å, and the 1280 cenwave at 1200 Å, 1300 Å, and 1400 Å. Several factors could explain those discrepancies: smearing of the observed XD profiles due to residual Y distortions in the image spectra, smearing of the XD profiles due to steep variations with wavelength relative to the binning value (500 pixels for the G140L). A specific, in-depth analysis of the XD profiles is required to fully understand and characterize their shape and its variations with wavelength and position on the detector.

We would expect the shape of the XD profiles to be for the most part determined by the PSF (and therefore the optics), and not by detector features. The comparison of the optical model and the observed profiles seems to support this conjecture. However, detector effects such as gain-sag and flat-fielding may create a dependency on detector position, and therefore FP-POS. The subtle variations between FPPOS seen in the observed XD profiles could suggest a contribution from detector effects, although it is not clear at this point whether these variations are statistically significant. A further analysis is required to draw conclusions on the repeatability and small scale variation of the XD profiles.

Lastly, the correspondence of the model and observed XD profiles provides an additional validation of the optical model, and therefore of the modeled LSFs of COS. Indeed, the XD profiles and LSFs are computed from the modeled PSF of the COS+OTA system.

5. Conclusion

We have modeled the COS FUV LSFs and XD profiles at lifetime position 2. The COS FUV model LSFs were validated using observations of SMC star AzV 75, by comparing ISM spectral line profiles identified in the observed COS spectra on the one hand, and synthetic COS spectra obtained from the convolution of archival STIS echelle E140M spectra with the model LSFs on the other hand. Our analysis shows the model of the LSFs characterizes the COS FUV spectral resolution very well: the residual between synthetic and observed COS spectra is within the error. We have made those model LSFs available to the community, at http://www.stsci.edu/hst/cos/performance/spectral_resolution/.

In addition, we have examined the COS FUV spatial resolution at lifetime position 2, using observations of white dwarves acquired as part of FCAL3 (PID 12806), as

a function of grating, cenwave, and wavelength. The optical model of the XD profiles provides a very good match to the observed XD profiles.

6. Recommendations

Improvements to the COS FUV optical model were made in this analysis. The improved optical model should be run at LP1 in order to properly assess the differences in resolution between LP1 and LP2.

Acknowledgements

J. Roman-Duval acknowledges helpful discussions with Gerard Kriss.

Change History for COS ISR 2013-07

Version 1: June 10, 2013- Original Document

References

- Ake, T., Massa, D., Beland, S., France, K., Penton, S., Sahnow, D., McPhate, J., 2010, HST calibration workshop, Susana Deustua and Cristina Oliveira, eds.
- Ghavamian, P. et al, COS Instrument Science Report 2009-01
- Krist, J.E., Hook, R.N., Stoehr, F., 2011, Proc. of SPIE: Optical Modeling and Performance Predictions V, Mark A. Kahan eds, Vol. 8127
- Oliveira et al. COS ISR 2013-01
- Sonnentrucker et al., COS ISR 2013-06
- Tumlinson, J., Shull, M., Rachford, B., et al., 2002, ApJ, 566, 857

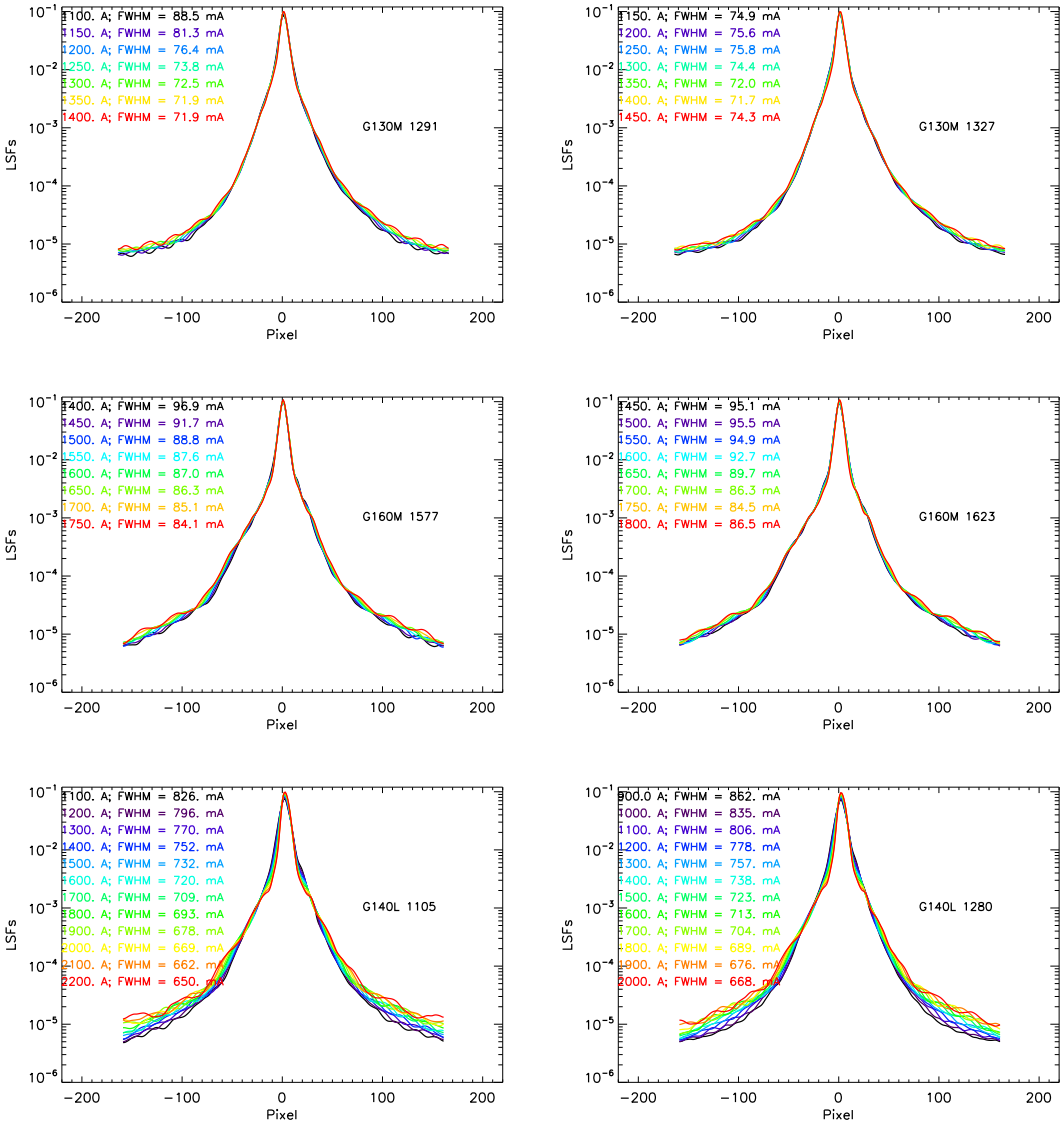

Figure 1.: *COS FUV LSFs for the extreme cenwaves of the G130M, G160M, and G140L. The corresponding grating and cenwave settings are indicated in each panel. For each grating/cenwave combination, the different colors correspond to different wavelengths, and the FWHM of the LSF is indicated in each panel for each wavelength.*

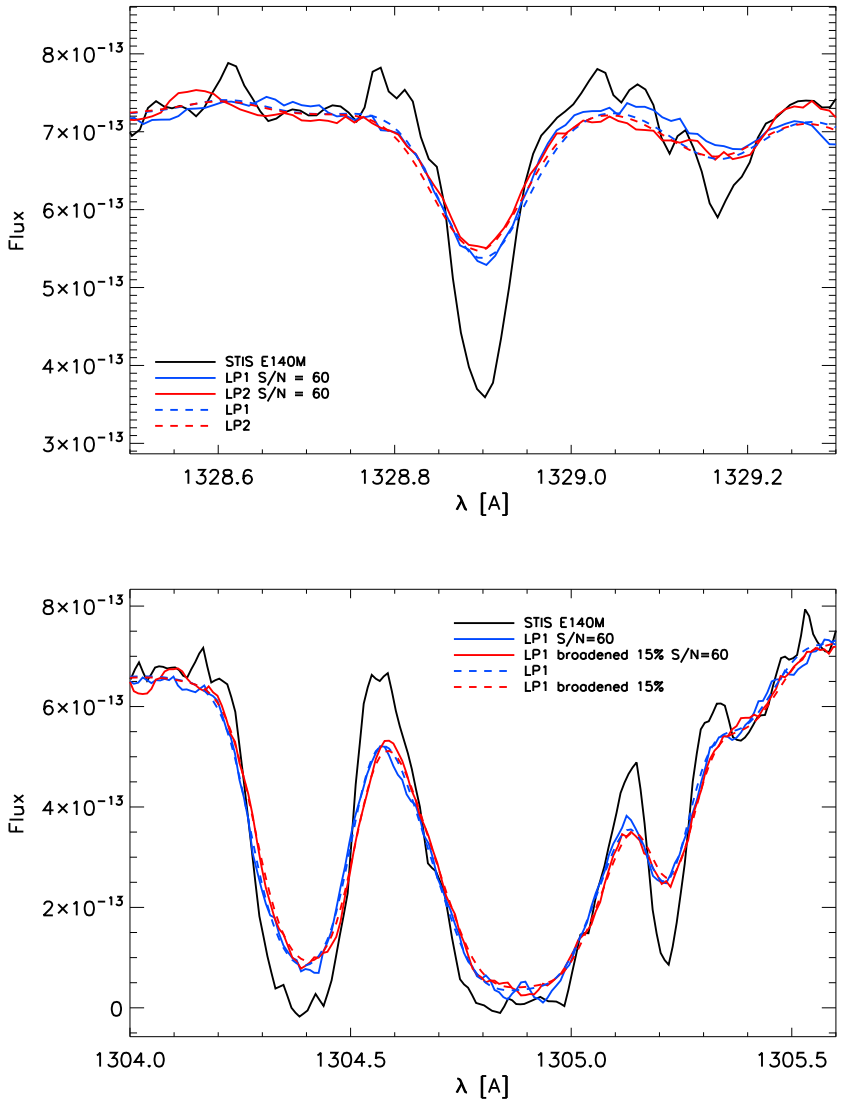

Figure 2.: *Comparison at 1328 Å (C I unresolved line, top) and at 1304 Å (Si II saturated profiles, bottom) between STIS E140M (black), and synthetic COS G130M spectra obtained with different methods. In the top panel, the synthetic COS spectra were obtained by convolving the STIS spectrum with the optical models of the COS LSFs at LP1 (blue) and LP2 (red). In the bottom panel, the synthetic COS spectra were obtained by convolving the STIS spectrum with COS FUV LSFs at LP1 (blue) on the one hand, and at LP1 broadened uniformly by 15% on the other hand (red). The convolution effectively averages out the noise in the high-resolution STIS spectrum, as seen in the dashed lines. Hence, gaussian noise with S/N = 60 per resolution element on the continuum was added to the synthetic spectrum, to obtain noisy synthetic spectra shown by the solid lines.*

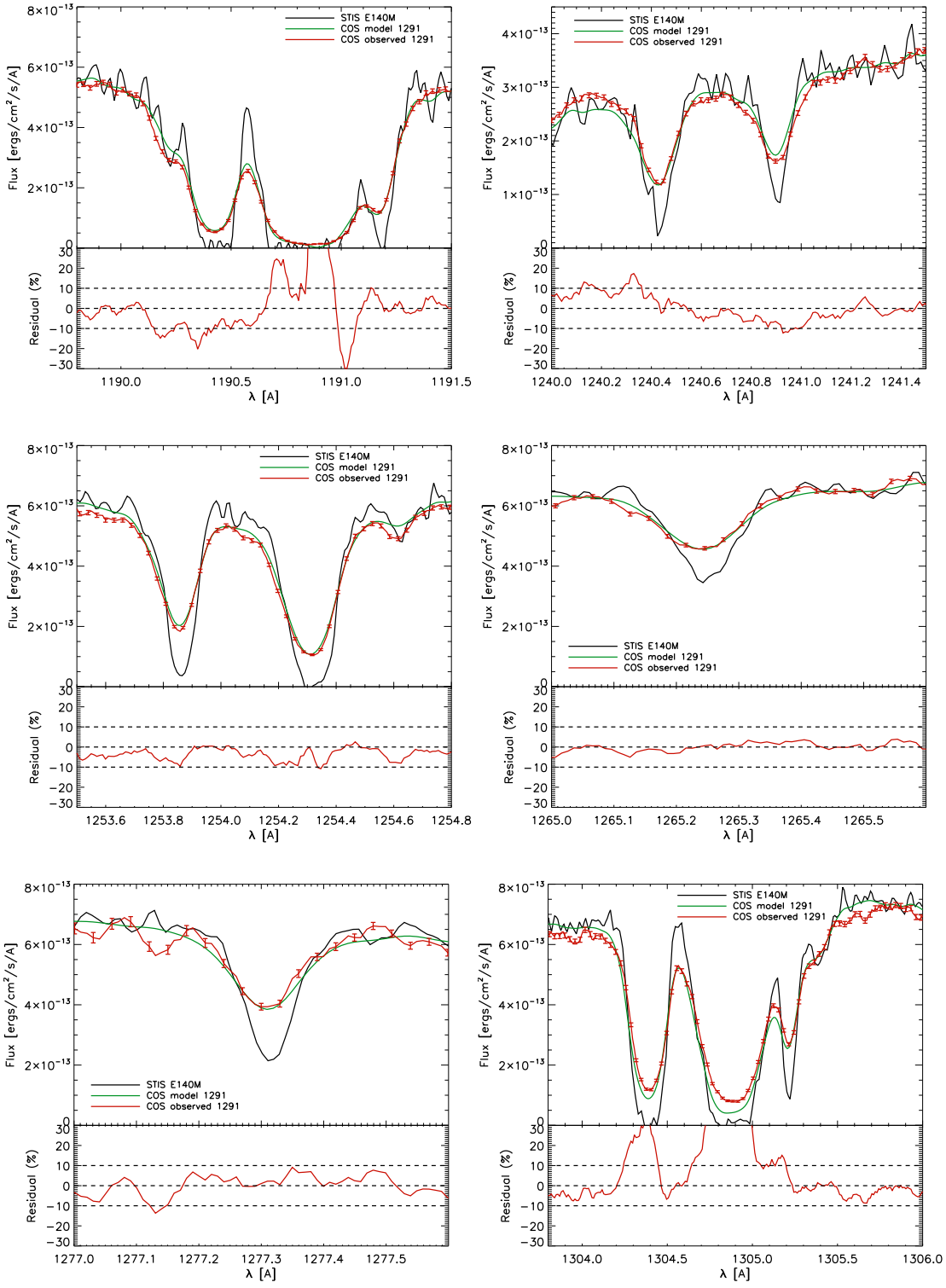
STIS E140M
COS model 1291
COS observed 1291
Flux [ergs/cm²/s/A]
Residual (%)
λ [A]

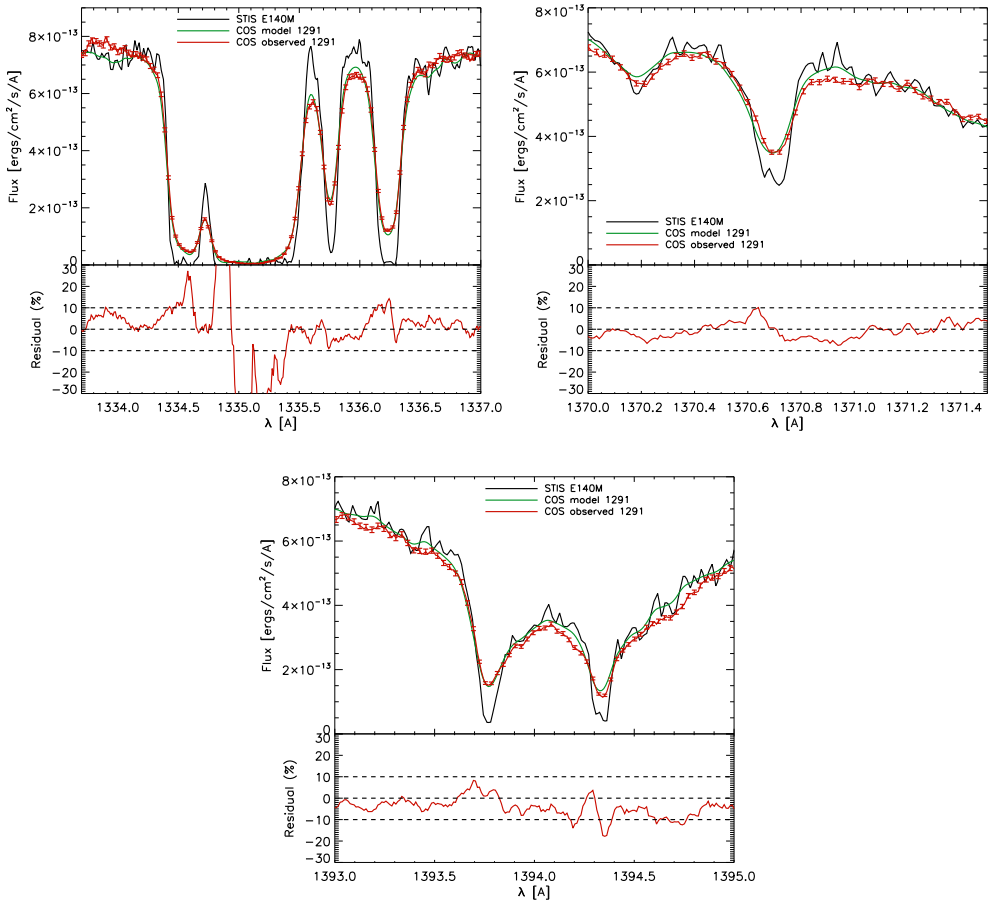

Figure 3.: *Comparison between COS synthetic (green) and observed (red) G130M/1291 spectra, in the wavelength range of various ISM lines observed in the G130M. The top panels correspond to the spectra, while the bottom panels show the residual, defined in Section , in %.*

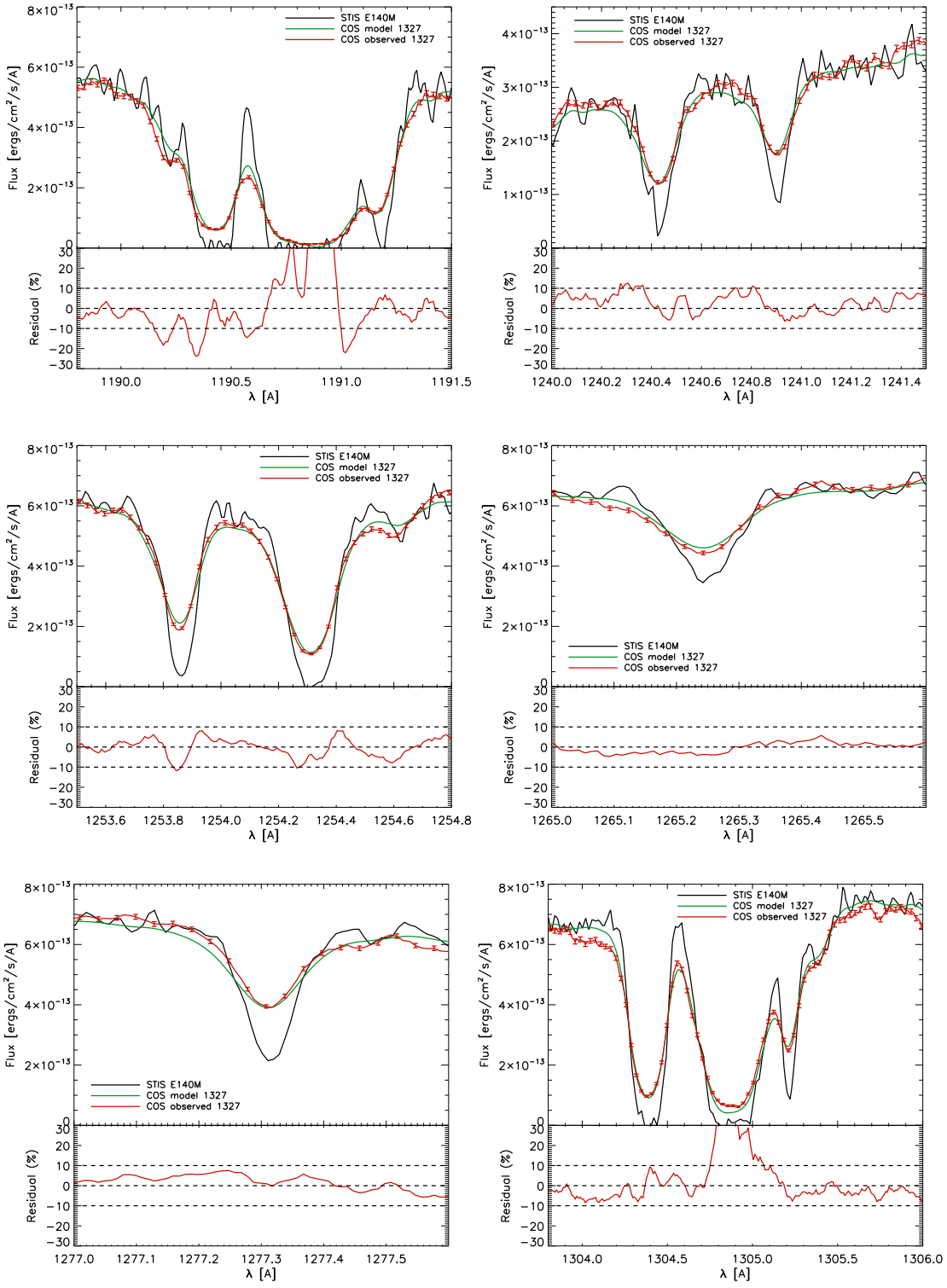
STIS E140M
COS model 1327
COS observed 1327
Flux [ergs/cm²/s/A]
Residual (%)
λ [A]

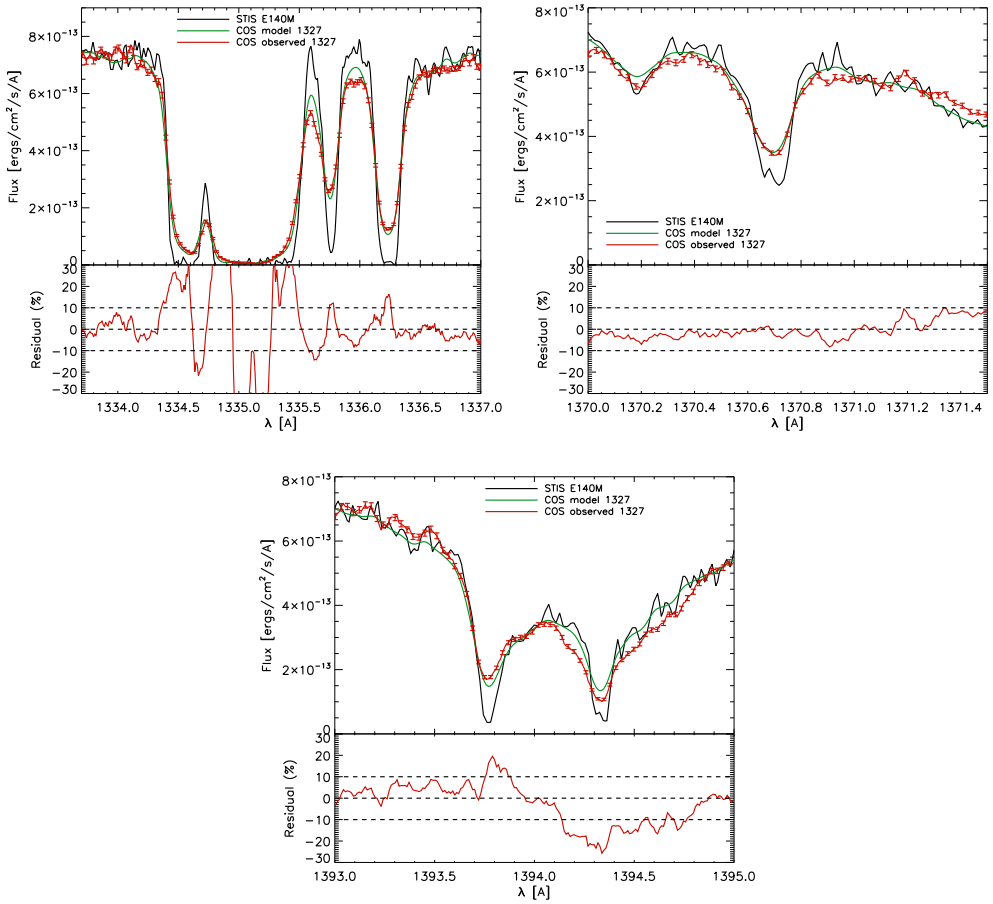

Figure 4.: *Comparison between COS synthetic (green)) and observed (red) G130M/1327 spectra, in the wavelength range of various ISM lines observed in the G130M. The top panels correspond to the spectra, while the bottom panels show the residual, defined in Section , in %.*

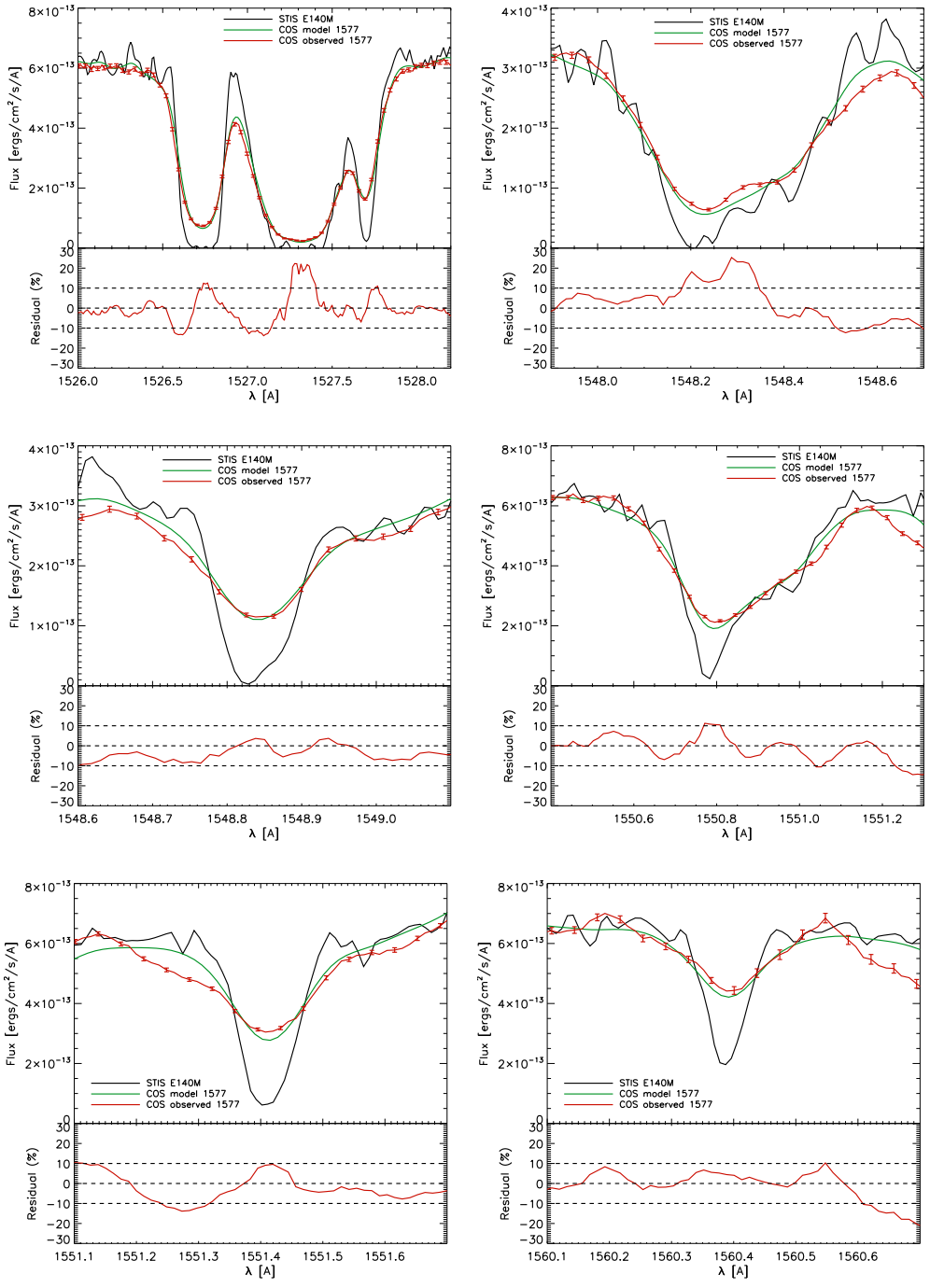
STIS E140M
COS model 1577
COS observed 1577
Flux [ergs/cm²/s/A]
Residual (%)
λ [A]

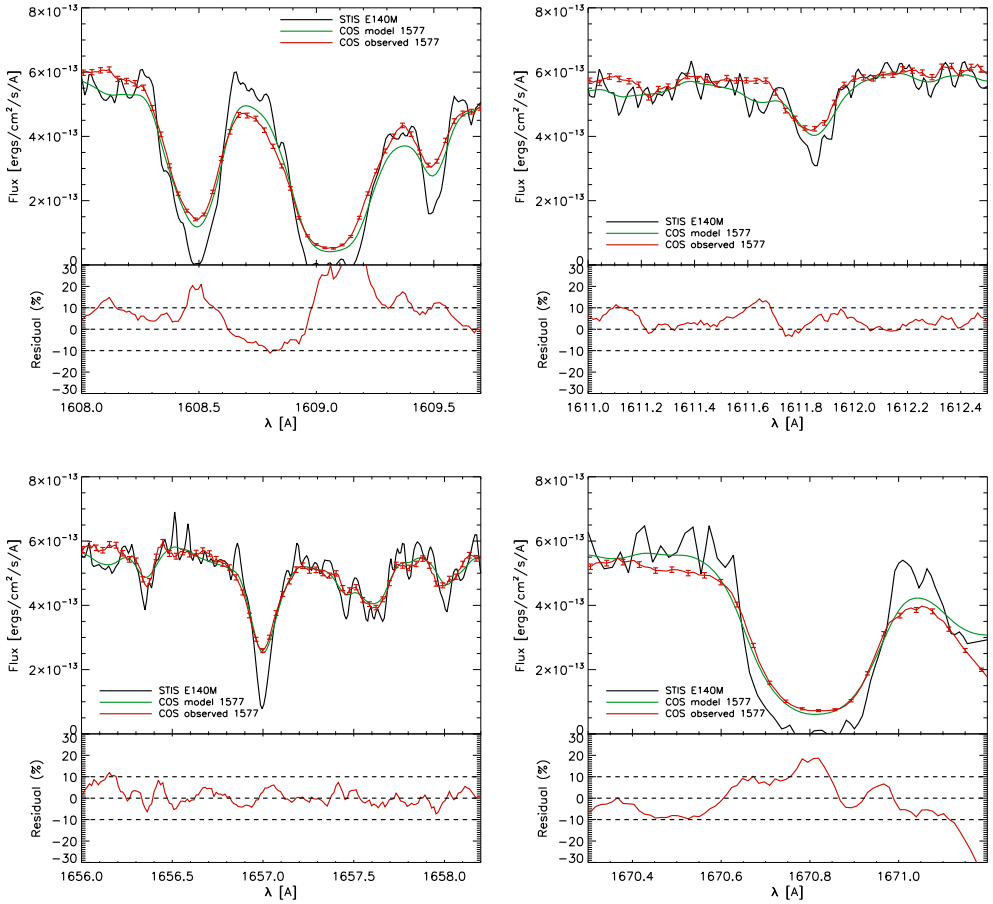

Figure 5.: *Comparison between COS synthetic (green) and observed (red) G160M/1577 spectra, in the wavelength range of various ISM lines observed in the G160M. The top panels correspond to the spectra, while the bottom panels show the residual, defined in Section , in %..*

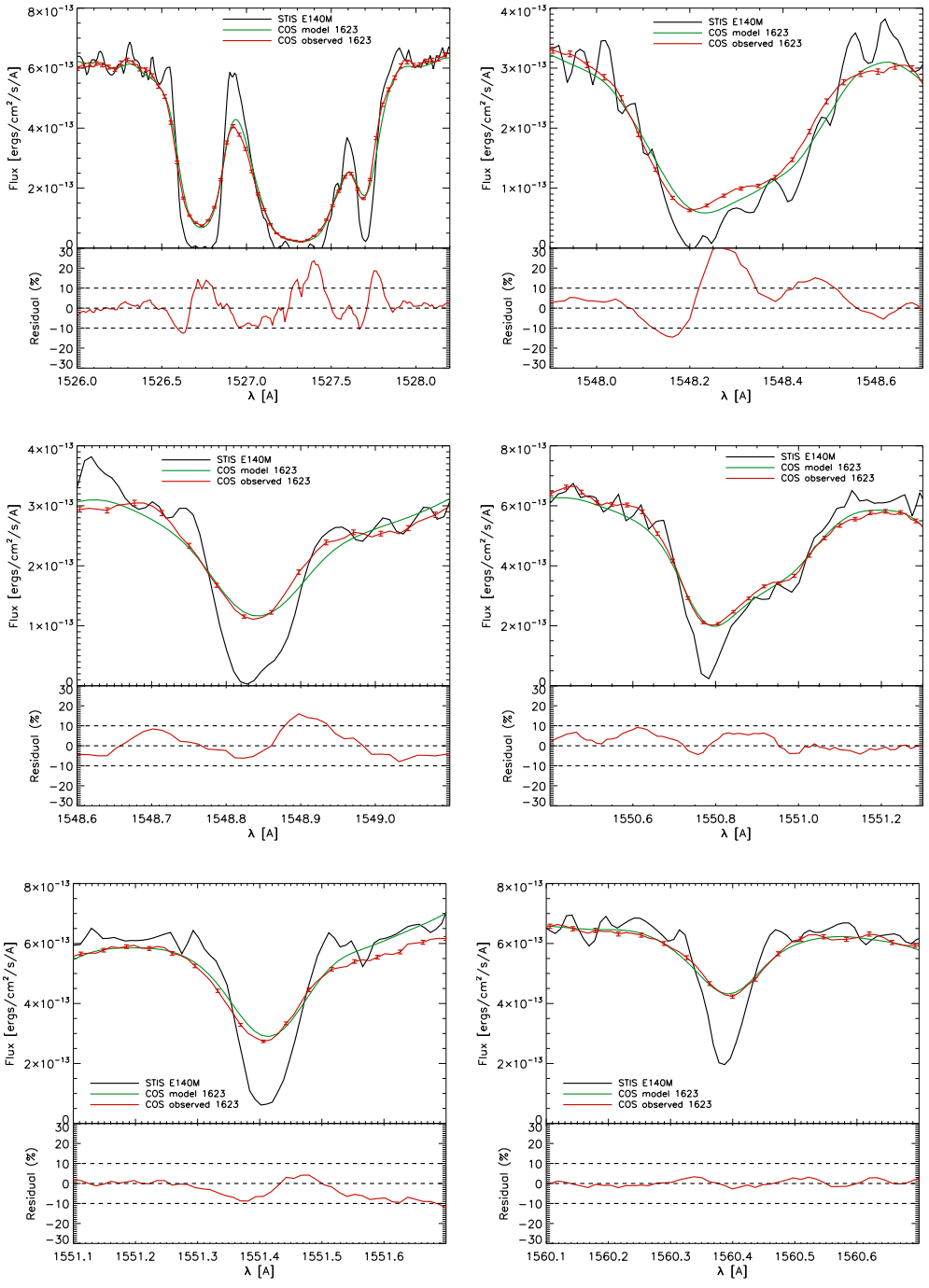
STIS E140M
COS model 1623
COS observed 1623
Flux [ergs/cm²/s/A]
Residual (%)
λ [A]

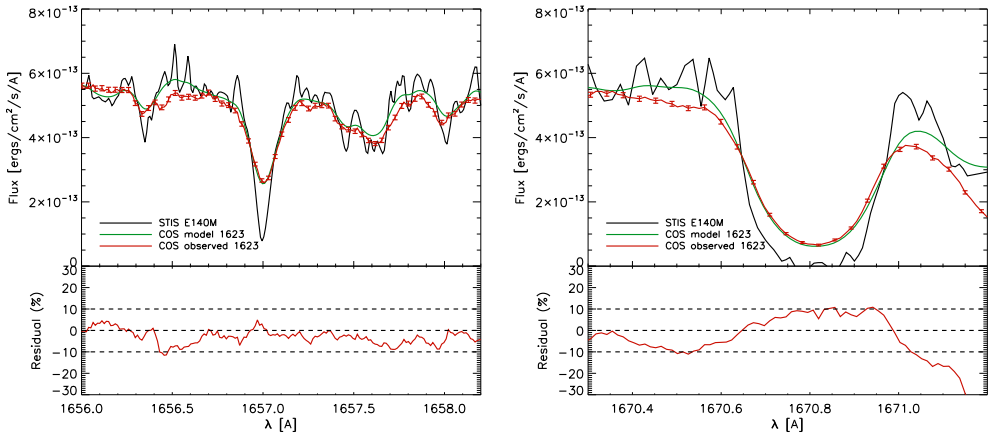

Figure 6.: *Comparison between COS synthetic (green) and observed (red) G160M/1623 spectra, in the wavelength range of various ISM lines observed in the G160M. The top panels correspond to the spectra, while the bottom panels show the residual, defined in Section , in %.*. Note that the 1608-1612 Å range is not covered by the G160M/1623 cenwave, since it falls in the gap.

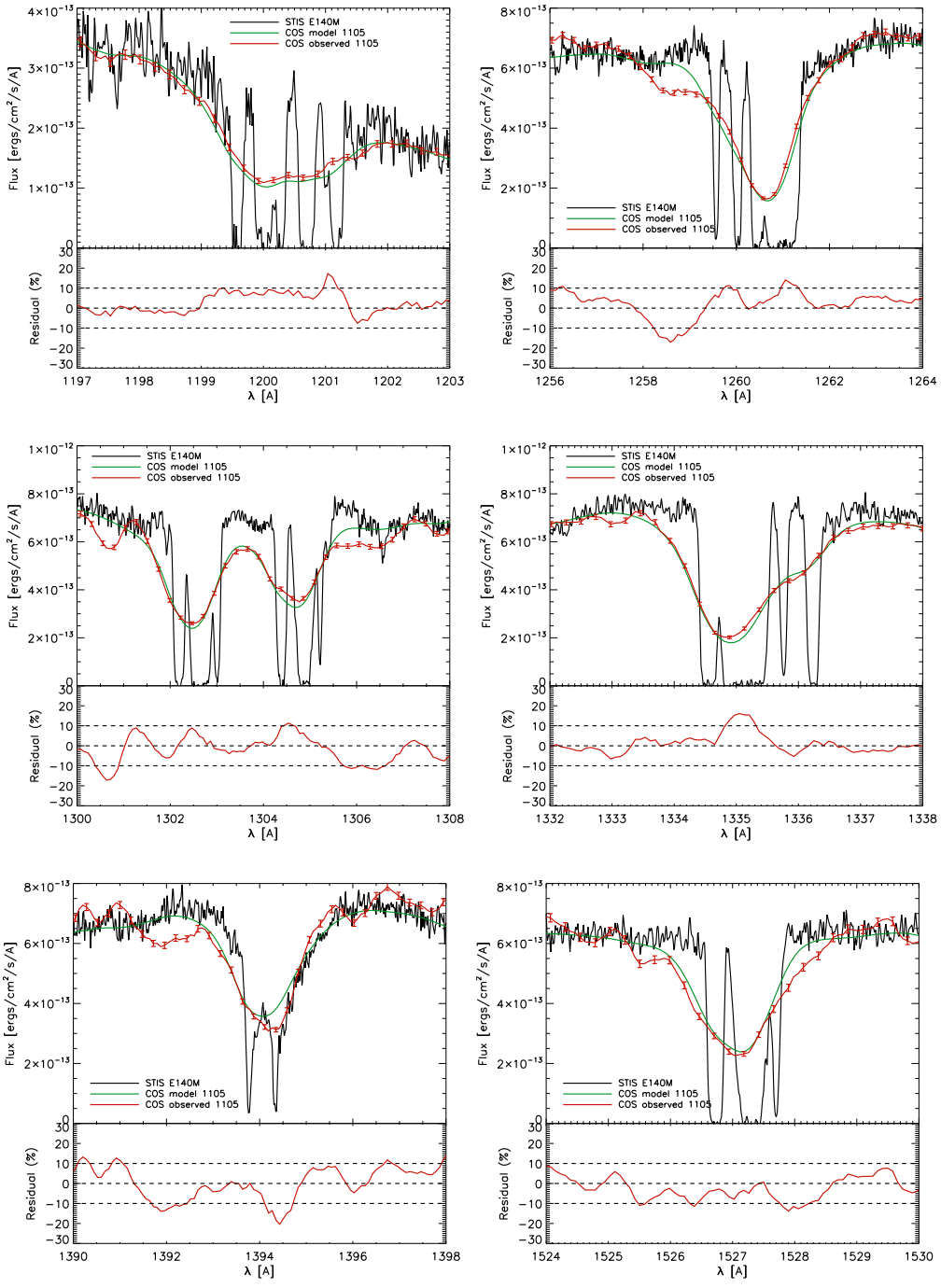
STIS E140M
COS model 1105
COS observed 1105
Flux [ergs/cm²/s/A]
Residual (%)
λ [A]

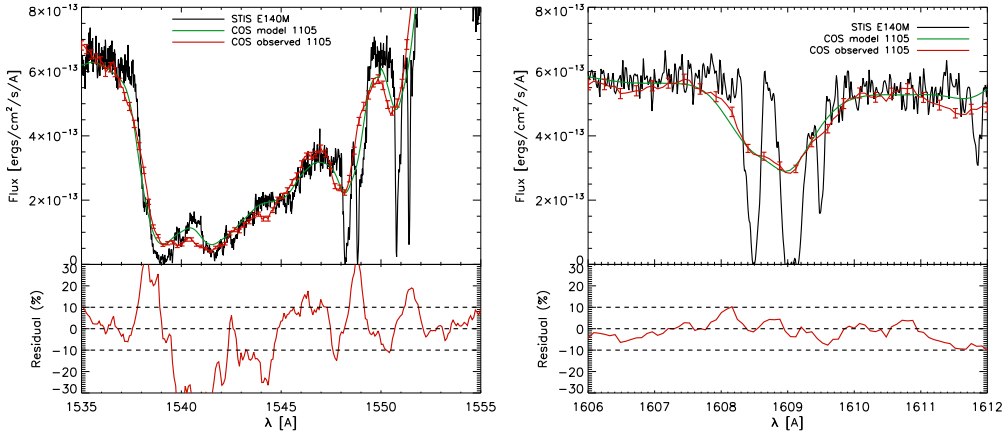

Figure 7.: *Comparison between COS synthetic (green) and observed (red) G140L/1105 spectra, in the wavelength range of various ISM lines observed in the G140L. The top panels correspond to the spectra, while the bottom panels show the residual, defined in Section , in %.*

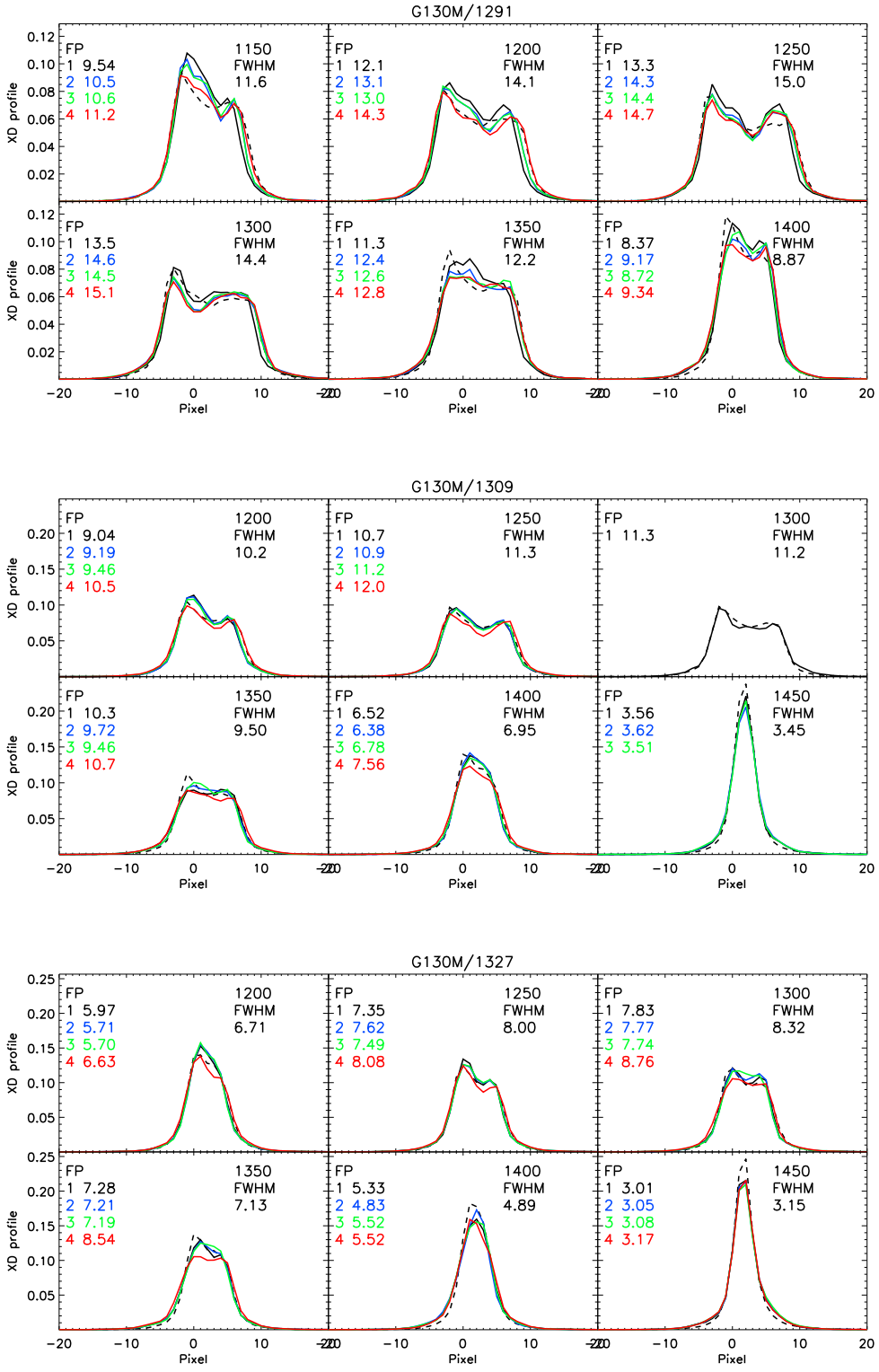

Figure 8.: *Comparison between observed (solid lines, one color per FP-POS) and modeled (dashed lines) XD profiles for the 1291 (top), 1309 (middle), and 1327 (bottom) cenwaves of the G130M, as a function of wavelength. The FWHM of the profiles, in units of pixels, are indicated in each panel, on the left and right sides for the observed and model XD profiles respectively.*

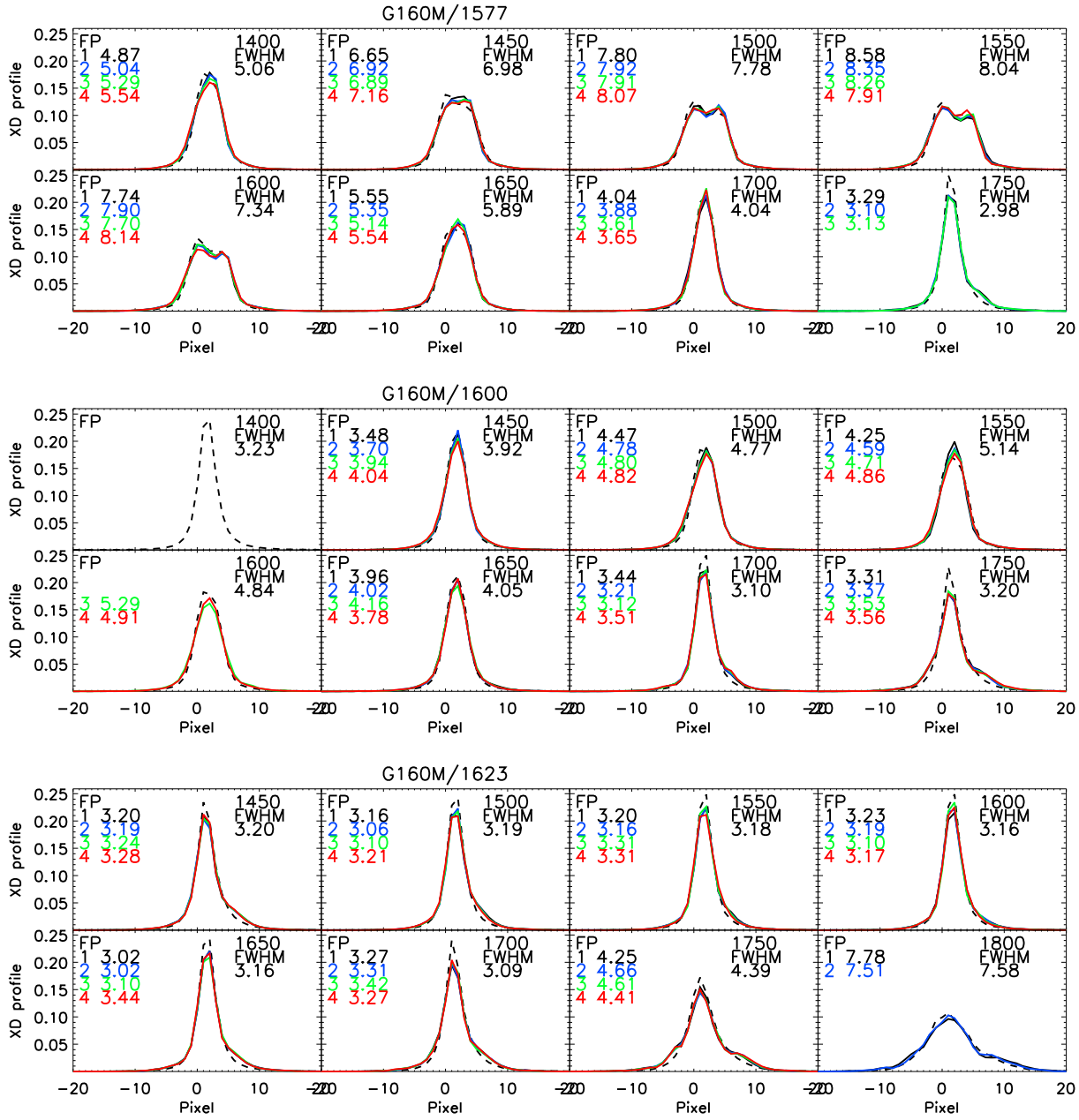

Figure 9.: *Comparison between observed (solid lines, one color per FP-POS) and modeled (dashed lines) XD profiles for the 1577 (top), 1600 (middle), and 1623 (bottom) cenwaves of the G160M, as a function of wavelength. The FWHM of the profiles, in units of pixels, are indicated in each panel, on the left and right sides for the observed and model XD profiles respectively.*

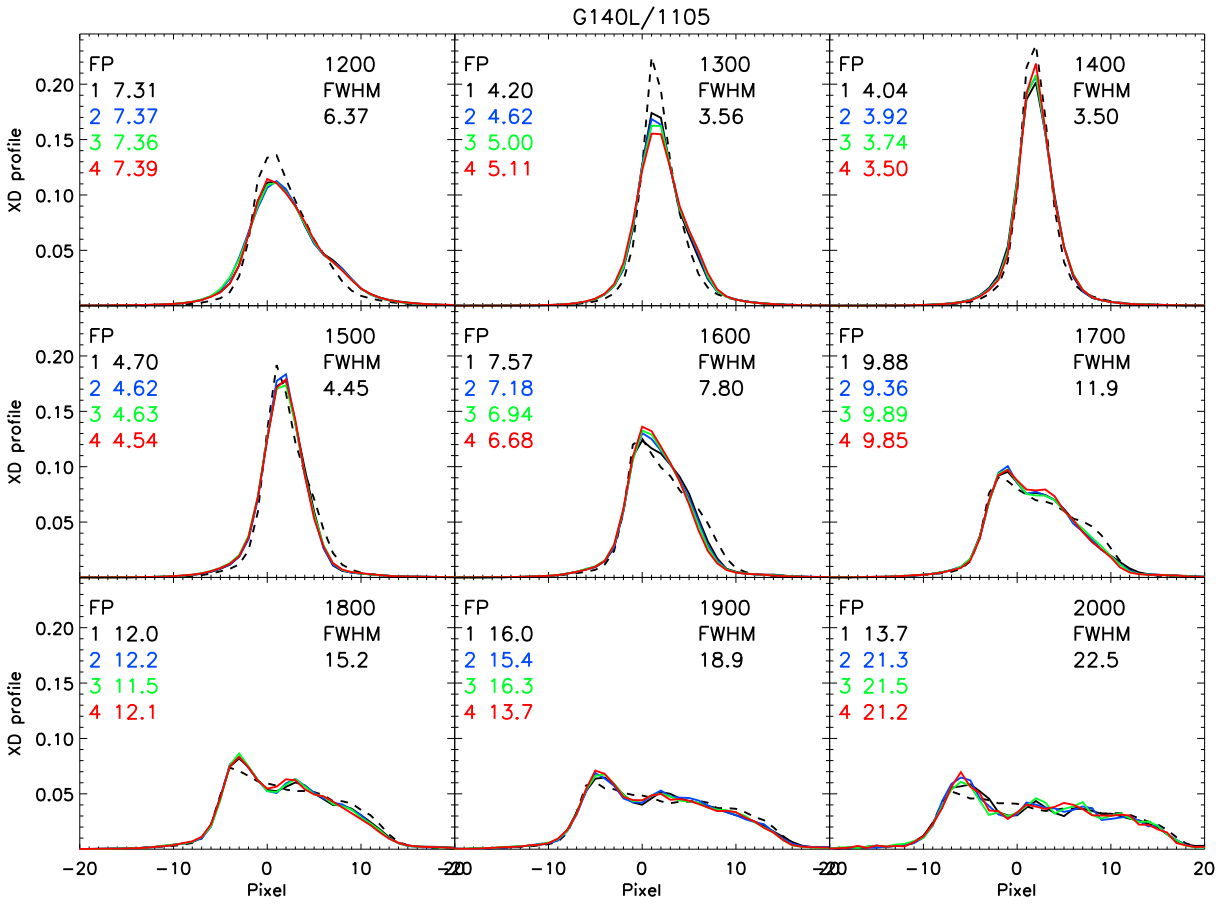
G140L/1105
FP
1 7.31
2 7.37
3 7.36
4 7.39
1200
FWHM
6.37
FP
1 4.20
2 4.62
3 5.00
4 5.11
1300
FWHM
3.56
FP
1 4.04
2 3.92
3 3.74
4 3.50
1400
FWHM
3.50
FP
1 4.70
2 4.62
3 4.63
4 4.54
1500
FWHM
4.45
FP
1 7.57
2 7.18
3 6.94
4 6.68
1600
FWHM
7.80
FP
1 9.88
2 9.36
3 9.89
4 9.85
1700
FWHM
11.9
FP
1 12.0
2 12.2
3 11.5
4 12.1
1800
FWHM
15.2
FP
1 16.0
2 15.4
3 16.3
4 13.7
1900
FWHM
18.9
FP
1 13.7
2 21.3
3 21.5
4 21.2
2000
FWHM
22.5
XD profile
Pixel

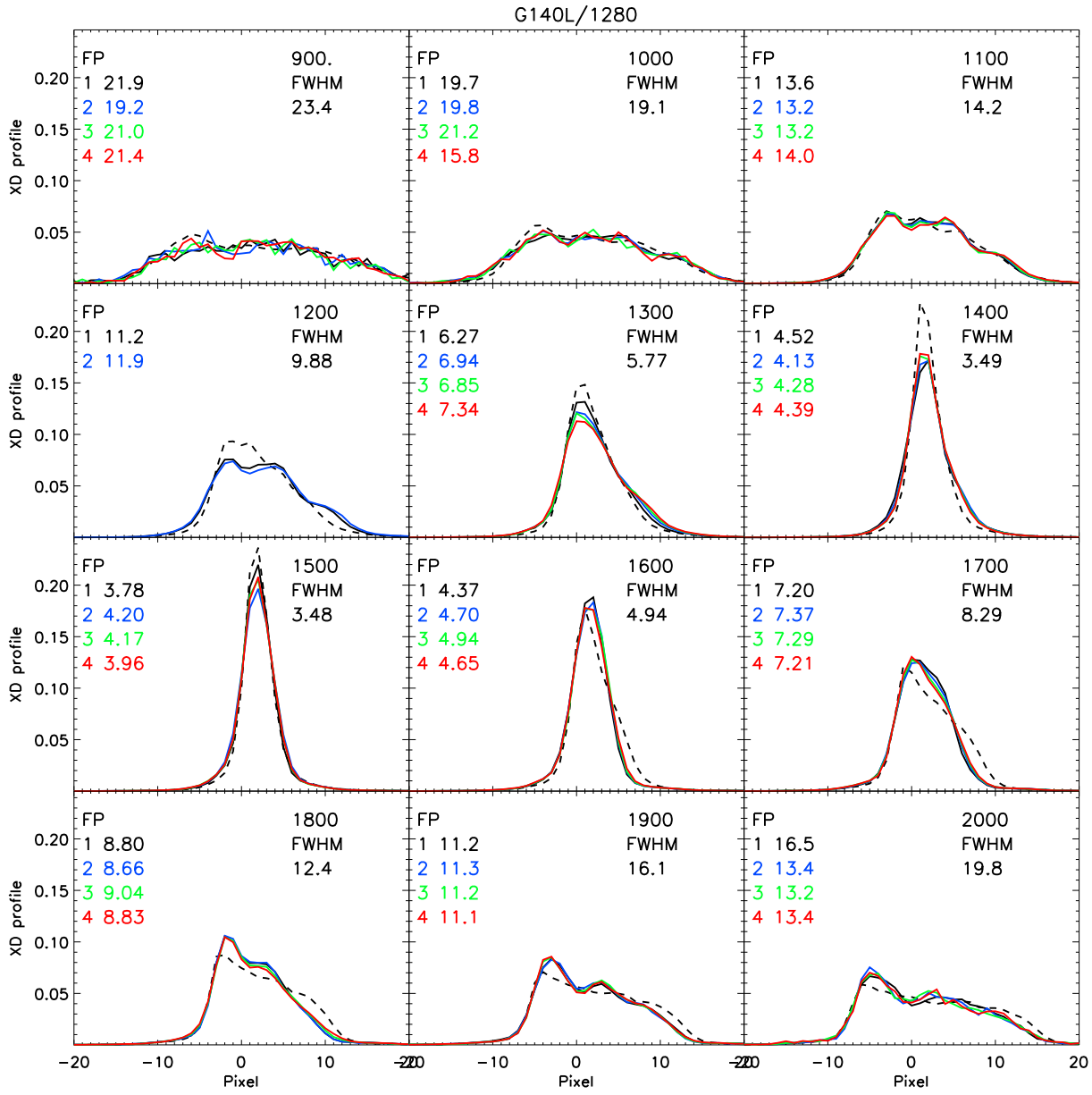

Figure 10.: *Comparison between observed (solid lines, one color per FP-POS) and modeled (dashed lines) XD profiles for the 1105 (top) and 1280 (bottom) cenwaves of the G140L, as a function of wavelength. The FWHM of the profiles, in units of pixels, are indicated in each panel, on the left and right sides for the observed and model XD profiles respectively.*

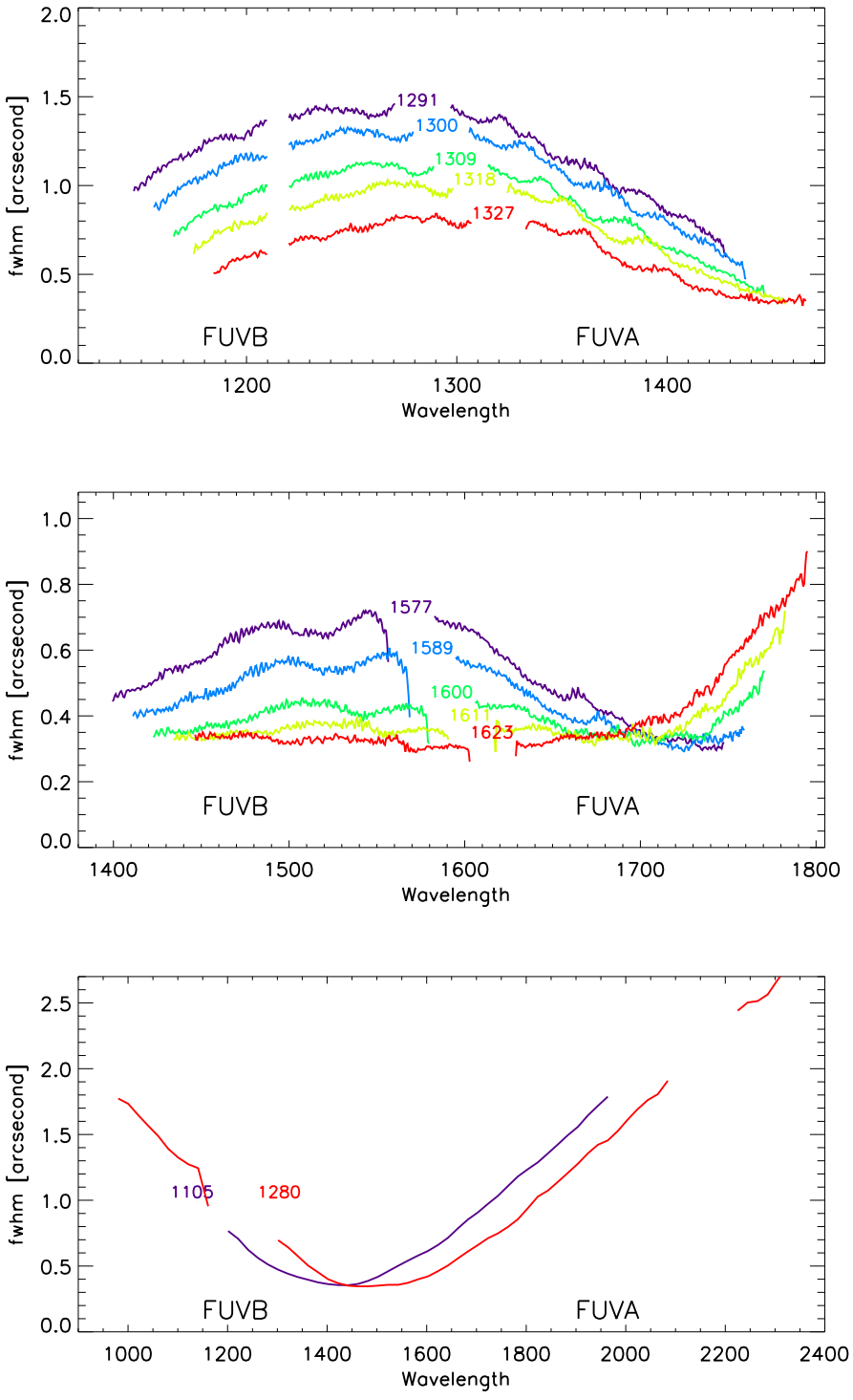

Figure 11.: *Measured spatial resolution (FWHM of the XD profile) of the G130M (top), G160M (middle), and G140L (bottom) as a function of wavelength for segment B and A and the different cenwaves. The XD profile was obtained by binning the image spectrum along dispersion by 100 pixels for the M gratings, and 500 pixels for the G140L. The FWHM is shown in units of arc seconds. The plate scale is 0.1 arc second per pixel.*

Table 5. *Exposures from 12806 (FCAL3) used in the characterization of the spatial resolution of the COS FUV gratings.*

LP	Grating	Cenwave	Exposure	FP-POS
LP2	G130M	1291	lbxm1aq6q	1
			lbxm1aqdq	2
			lbxm1aqfq	3
			lbxm1aqpq	4
			lbxmt3m3q	3
		1300	lbxm1burq	1
			lbxm1bv3q	2
			lbxm1bv7q	3
			lbxm1bv9q	4
		1309	lbxm1aqrq	1
			lbxm1aqtq	2
			lbxm1aqvq	3
			lbxm1ar4q	4
			lbxmt3m1q	3
		1318	lbxm1bvbq	1
			lbxm1bviq	2
			lbxm1bvkq	3
			lbxm1bvmq	4
		1327	lbxm1ar6q	1
			lbxm1ar8q	2
			lbxm1araq	3
			lbxm1arcq	4
			lbxmt3mcq	3
	G160M	1577	lbxm02aaq	1
			lbxm02acq	2
			lbxm02agq	3
			lbxm02alq	4
			lbxm03fgq	1
			lbxm03fkq	2
			lbxm03fmq	3
			lbxm03foq	4
			lbxmt4loq	3
		1589	lbxm02caq	1
			lbxm02ccq	2
			lbxm02ceq	3

Table 5. (cont'd)

LP	Grating	Cenwave	Exposure	FP-POS
LP2	G160M	1589	lbxm02cgq	4
			lbxm03fqq	1
			lbxm03fsq	2
			lbxm03fuq	3
			lbxm03fwq	4
		1600	lbxm02atq	1
			lbxm02avq	2
			lbxm02ayq	3
			lbxm02b0q	4
			lbxm03fyq	1
			lbxm03g0q	2
			lbxm03g2q	3
			lbxm03g4q	4
			lbxmt4mkq	3
		1611	lbxm02ciq	1
			lbxm02ckq	2
			lbxm02cwq	3
			lbxm02cyq	4
			lbxm03g6q	1
			lbxm03g8q	2
			lbxm03gaq	3
			lbxm03gcq	4
		1623	lbxm02btq	1
			lbxm02bvq	2
			lbxm02bxq	3
			lbxm02bzq	4
			lbxm03geq	1
			lbxm03ggq	2
			lbxm03giq	3
			lbxm03gkq	4
			lbxmt4mmq	3
	G140L	1105	lbxm1bvwq	1
			lbxm1bvyq	2
			lbxm1bw0q	3
			lbxm1bw2q	4

Table 5. (cont'd)

LP	Grating	Cenwave	Exposure	FP-POS
LP2	G140L	1105	lbxmt3mfq	3
		1280	lbxm1bvoq	1
			lbxm1bvqq	2
			lbxm1bvsq	3
			lbxm1bvuq	4
			lbxmt3lwq	3